ORIGINAL PAPER



Effects of APT20TTMG, a modulator of the U1 snRNP complex, in glioblastoma models

Caio Bruno Quinta de Souza Leal¹ · Camila Guimarães Moreira Zimmer¹ · Vanessa de Vasconcelos Castilho Sinatti¹ · Ericks Sousa Soares¹ · Michael S. Rafii² · Rafael Mantovani Bottos¹

Received: 20 May 2025 / Accepted: 17 September 2025 © The Author(s), under exclusive licence to Springer Science+Business Media, LLC, part of Springer Nature 2025

Abstract

The U1 small nuclear ribonucleoprotein (snRNP) complex is essential for pre-mRNA splicing and inhibition of premature polyadenylation. Its dysfunction has been implicated in various cancers, including glioblastoma, driving oncogenic splicing and tumor progression. This study explored the potential of APT20TTMG, a synthetic cDNA that modulates U1 snRNP misassembly, in glioblastoma. The internalization of APT20TTMG was assessed in U-87 MG cells, as well as its effects on cell viability, proliferation, and apoptosis. Athymic mice were used to evaluate the effects of intravenous APT20TTMG administration on tumor-related parameters. APT20TTMG exhibited over 50% internalization, exerting cytotoxic, cytostatic, and pro-apoptotic effects in vitro. A 22-day treatment with APT20TTMG reduced tumor volume, slowed tumor growth, and showed a trend toward increased body weight. Treatment also decreased oncogenic pathways and tended to enhance histopathological outcomes. A pilot study combining APT20TTMG with temozolomide further improved antitumor efficacy. Our results demonstrate that APT20TTMG has strong potential in correcting U1 snRNP complex dysfunction, supporting its further investigation as a strategy to modulate splicing in glioblastoma.

Keywords Antitumor therapy · Glioblastoma · Subcutaneous xenograft model · U1 snRNP complex · U-87 MG

Introduction

Glioblastoma (GBM) is the most common and aggressive primary brain tumor, classified by the World Health Organization as a grade IV CNS malignancy [1, 2]. It is associated with a poor prognosis, with a median survival of 12–16 months following diagnosis [3]. The current standard of care includes surgical resection, radiotherapy, and chemotherapy with temozolomide (TMZ). However, GBM exhibits high resistance, especially due to the isocitrate dehydrogenase (IDH) wildtype genotype, which promotes cellular heterogeneity and contributes to resistance against standard therapies and tumor recurrence [4–7].

Rafael Mantovani Bottos rbottos@aptah-bio.com

Published online: 02 October 2025

Alternative polyadenylation is a critical process in the progression of GBM and other cancer types [8–11]. Although it increases transcript diversity [12], cancer cells tend to use proximal polyadenylation signals, resulting in shorter 3' untranslated regions and higher protein expression levels, which has been associated with increased proliferation [10, 13]. Additionally, spliceosome alterations in GBM drive oncogenic splicing events that promote tumor progression, TMZ resistance, and could be involved with cell cycle reentry [14–17]. Dysregulated expression of spliceosome components, such as small nuclear ribonucleoproteins (snRNPs), has also been observed [17].

The U1 snRNP complex, composed of a U1 snRNA and U1-A, U1-C, U1-70K, and Sm proteins, is a key regulator of both splicing and polyadenylation. It recognizes splicing sites and facilitates spliceosome assembly through its binding to the 5' splicing site [18], as well as prevents premature cleavage and polyadenylation of pre-mRNAs, thereby maintaining transcripts integrity [19]. By regulating alternative polyadenylation patterns, it acts as a molecular safeguard against aberrant gene expression and pro-oncogenic signaling. Consequently, targeting the U1 snRNP complex to



Aptah Bio Inc., 930 Brittan Avenue, San Carlos, CA 94070, USA

Alzheimer's Therapeutic Research Institute, University of Southern California, 9860 Mesa Rim Road, San Diego, CA 92121, USA

507 Page 2 of 11 Medical Oncology (2025) 42:507

restore its function represents a promising therapeutic strategy for correcting pathological alterations driven by splicing and polyadenylation dysregulation.

In this study, we evaluated the effects of APT20TTMG in GBM models. It is a synthetic single-stranded cDNA designed through computer-aided design strategies to contain precise chemical modifications, sequence specificity, and structural features that enable its binding to U1 snRNPs and conserved regions of pre-mRNAs [20]. These APT20TTMG interactions ensure the proper assembly and function of the U1 snRNP complex, effectively restoring normal splicing and polyadenylation mechanisms.

Methods

Drugs

APT20TTMG was synthesized by Synbio Technologies (Monmouth Junction, NJ, USA) and stored at - 20 °C until use. For in vitro experiments, APT20TTMG (batches P20190506-11 for internalization, P20190717-11 for viability, P20201023-12 for proliferation, and P20190924-08 for apoptosis) was reconstituted in deionized water or phosphate-buffered saline (PBS) to prepare a 300 µM stock solution. This stock solution was subsequently diluted to achieve final concentrations of 0.003, 0.03, 0.3, 3, and 30 µM. Cisplatin (Clearsynth, Mumbai, India) was prepared by reconstitution in a mixture of dimethyl sulfoxide (Rankem, Gurugram, India) and water, with stock solutions diluted to final concentrations of 0.01, 0.1, 1, and 10 µM. For in vivo experiments, 5 mg of APT20TTMG (batch 20220803002–1) was diluted in 1.25 ml of saline to achieve a concentration of 4 mg/ml. A dose volume of 5 ml/kg was administered via intravenous (i.v.) to deliver a final dose of 20 mg/kg. For TMZ (Sigma-Aldrich, St. Louis, MO, USA), 1.5 mg of the compound was solubilized in a solution containing 4% Tween 80 in distilled water to obtain a uniform suspension of 0.5 mg/ml. A dose volume of 10 ml/kg was administered orally (p.o.) to achieve a final dose of 5 mg/kg.

Cell culture

Human GBM U-87 MG cells, acquired from the American Type Culture Collection (Manassas, VA, USA), were cultured in 75 cm² flasks using Dulbecco's Modified Eagle Medium (HiMedia Laboratories, Thane, India) supplemented with 10% fetal bovine serum (FBS; Sigma-Aldrich, St. Louis, MO, USA) and 1% penicillin/streptomycin solution (Gibco, Grand Island, NY, USA). Cells were maintained in a humidified incubator at 37 °C with 5% CO₂. Before plating, cells were counted using a hemocytometer (Hausser Scientific, Horsham, PA, USA).



Cells were plated in 24-well plates (1×10^5 cells/well) and incubated with 1 μ M FAM-labeled APT20TTMG, prepared in FBS-free medium, for 1, 2, 4, and 6 h. Vehicle-incubated cells were used as controls. Following incubation, wells were washed twice with 1 ml of PBS/well and incubated with 200 μ L of trypsin (Sigma-Aldrich, St. Louis, MO, USA) for 3 min. Trypsin was neutralized by adding complete medium and the cells were centrifuged at 1500 rpm for 5 min. The cell pellet was then washed with 2 ml of PBS and centrifuged as previously. After discarding the supernatant, the cells were resuspended in 200 μ L of PBS. Cellular uptake of APT20TTMG was assessed by measuring cell fluorescence using the BD FACSCanto II flow cytometer (BD Biosciences, Franklin Lakes, NJ, USA). For each sample, 10,000 gated events were acquired.

Cell viability

Cells were plated in 96-well plates (5×10^3 cells/well) and treated with APT20TTMG ($0.003,\,0.03,\,0.3,\,3.$, or $30\,\mu\text{M}$) or cisplatin ($0.01,\,0.1,\,1.$, or $10\,\mu\text{M}$) in 1% FBS medium, for 48, 96, and 144 h. Cells treated with dimethyl sulfoxide/water were used as a control. After 48 h, APT20TTMG or cisplatin were re-added to the wells until the end of the assay. At each time-point, the medium was replaced with fresh medium containing 20 μ L of MTT solution (5 mg/ml; Invitrogen, Waltham, MA, USA) for 3 h at 37 °C. Absorbance was measured at 540 nm using the Synergy H1 microplate reader (BioTek, Winooski, VT, USA). Results were normalized to the percentage of viability relative to the control. The maximum inhibitory effect (I_{max}) of APT20TTMG was determined using log(inhibitor) vs. normalized response analysis.

Cell proliferation

Cells were plated in 96-well plates (2×10^3 cells/well) and treated as previously described, and proliferation was determined at 48, 96, and 144 h using the bromodeoxyuridine (BrdU) incorporation assay (Roche, Basel, Switzerland). Cells were incubated with 10 μ L of BrdU for 90 min at 37 °C. The medium was then replaced with 200 μ L of FixDenat solution, followed by a 30-min incubation at room temperature. After removing FixDenat, 100 μ L of Anti-BrdU-POD solution was added and cells were incubated for 90 min at room temperature. The wells were washed three times with 20 μ L of washing solution and 100 μ L of substrate solution was added for 30 min at room temperature. Absorbance was measured at 370 nm using the Synergy HT



Medical Oncology (2025) 42:507 Page 3 of 11 507

microplate reader (BioTek, Winooski, VT, USA). Results were normalized to the percentage of proliferation relative to the control. The I_{max} of APT20TTMG was determined using log(inhibitor) vs. normalized response analysis.

Apoptosis

The apoptosis-inducing potential of APT20TTMG was evaluated using the Annexin V Apoptosis Detection kit (eBio-Science, San Diego, CA, USA). Cells were plated in 24-well plates (1×10^5 cells/well) and treated with APT20TTMG (0.25, 0.5, and 1 μ M) for 24 h. Cells were then collected as previously described and washed with PBS and binding buffer. Cells were labeled with fluorescein isothiocyanate-conjugated annexin V for 15 min, washed again with binding buffer, and then stained with propidium iodide. Apoptosis was analyzed using the BD FACSCanto II flow cytometer (BD Biosciences, Franklin Lakes, NJ, USA). For each sample, 10,000 gated events were acquired.

Animals

Female athymic nude mice (Vivo Bio Tech, Hyderabad, India), aged 6-8 weeks, were housed in individually ventilated cages under pathogen-free conditions, controlled temperature (19.1–21.8 °C, 40–61% relative humidity), and a 12-h light/dark cycle. Food and filtered sterile water were provided ad libitum. All in vivo experiments were conducted at the Dabur Research Foundation (Ghaziabad, India) in accordance with their ethical standards. Procedures adhered to the Animal Research: Reporting of In Vivo Experiments guidelines. The study was approved by the Institutional Animal Ethics Committee (IAEC/79/1532) and authorized by the Committee for the Purpose of Control and Supervision of Experiments on Animals (CPCSEA; registration no. 64/PO/RcBi/S/99/CPCSEA, dated 28.02.22). The use of APT20TTMG was approved by the Institutional Biosafety Committee (BT/BS/17/775/2018-PID; no. IBSC/12/005).

Subcutaneous xenograft model

Human GBM U-87 MG cells were maintained in Eagle's Minimum Essential Medium (Sigma-Aldrich, St. Louis, MO, USA) supplemented with 10% FBS. Log-phase cells were harvested using trypsin, washed with Eagle's Minimum Essential Medium, and resuspended at a concentration of 10 million cells / 100 μL in serum-free medium. Cells were mixed 1:1 with Matrigel matrix and 200 μL of the mixture was injected into the right flank of five donor mice. Tumor growth was monitored on alternate days and once the tumor reached 500 mm³, the mice were euthanized. Tumors were fragmented into 30 mg pieces and implanted

subcutaneously (s.c.) into experimental animals (n=45) using trocar devices.

Animals were monitored for tumor growth twice weekly and once the tumor reached 100 mm³, they were randomized (n = 8/group) into the following groups: vehicle (5 ml/kg saline, i.v., every third day for three weeks), TMZ (5 mg/kg, p.o., daily for three weeks), and APT20TTMG (20 mg/kg, i.v., every third day for three weeks). The sample size was based on previous studies, which demonstrated sufficient statistical power to detect significant effects. In a pilot study (n = 5/group), mice were treated with APT20TTMG (10 or 20 mg/kg, i.v.) alone or combined with TMZ (5 mg/kg, p.o., daily). The pilot treatment regimen with APT20TTMG included an initial 7-day attack dose (daily), followed by a maintenance dose (every three days), and a final 7-day attack dose, totaling 30 days. Mice without tumors or with aggressive tumor growth were excluded. Tumor size (length and width) was measured using a digital vernier caliper (Mitutoyo, Kawasaki, Japan). Body weight and clinical signs were recorded weekly.

At the end of treatments, mice were euthanized by CO_2 asphyxiation. In the pilot study, all mice of the vehicle group and three mice from each treatment group were euthanized on day 22, while the remaining animals continued treatment until day 30. Tumors were dissected, weighed, and divided into two portions: one fixed in 10% neutral buffered formalin and the other snap-frozen and stored at -80 °C for histopathological analysis.

Histopathology

Tumor sections on slides were deparaffinized in two xylene baths (5 min each) and rehydrated through a graded alcohol series (two baths of 100% alcohol, one of 95%, and one of 80%, 3 min each). Heat-induced epitope retrieval was performed using citrate buffer (pH 6.0) at 95 °C for 20 min to prevent methylene bridges formation. Slides were rinsed three times with PBS, incubated with peroxidase for 10 min, and blocked with blocking solution for 5 min. They were then incubated with the Ki-67 antibody (1:200; Zytomed Systems, Berlin, Germany) for 60 min, followed by three washes and incubation with poly-HRP-streptavidin conjugate for 30 min. After additional washes, slides were incubated with 3,3'-diaminobenzidine solution for 5 min, rinsed with distilled water, counterstained with hematoxylin and eosin, and mounted. Images were acquired using a Diaphot 300 microscope (Nikon, Tokyo, Japan). Ki-67-positive cells were quantified using the ImageJ software (NIH, USA). Additional histopathological parameters, including nucleus-to-cytoplasm (N:C) ratio, apoptosis, necrosis, capsule, and angiogenesis, were analyzed. According



507 Page 4 of 11 Medical Oncology (2025) 42:507

to these parameters, samples were classified into three grades: 1 < 25% anaplastic cells – well-differentiated), 2 < 25-50% anaplastic cells), and 3 < 50-75% anaplastic cells – less differentiated).

Biomarkers

For quantification of protein kinase B (AKT), glial fibrillary acidic protein (GFAP), TAU, cyclic adenosine 3′, 5′-monophosphate (cAMP), nuclear factor kappa B (NF-kB), and transforming growth factor-beta 1 (TGF-β), tumor tissues were homogenized and centrifuged. The supernatant was collected and analyzed using the following ELISA kits: Human AKT Protein (MyBioSource, San Diego, CA, USA), Human GFAP (Cusabio, Houston, TX, USA), Human TAU Protein (MyBioSource, San Diego, CA, USA), cAMP (MyBioSource, San Diego, CA, USA), Human NF-kB (MyBioSource, San Diego, CA, USA), and Human TGFB1 (Abbexa, Cambridge, UK) ELISA kits.

Statistical analysis

For in vitro data (two or three independent experiments with two or three technical replicates), one-way ANOVA, followed by Dunnett's multiple comparison test, was used. For in vivo data, one- or two-way ANOVA, followed by Dunnett's or Tukey's multiple comparisons tests, were used. Statistical significance was set as p < 0.05. Data were analyzed using the GraphPad Prism 10 software (GraphPad Software Inc., San Diego, CA, USA) and expressed as mean \pm standard error of the mean (SEM).

Results

APT20TTMG shows time-dependent internalization

A significant increase in the internalization of APT20TTMG in U-87 MG cells was observed over time (Supplementary Fig. S1), with rates of $47.4\pm4.7\%$ at 1 h, $45.4\pm3.9\%$ at 2 h, $58.0\pm4.8\%$ at 4 h, and $63.6\pm3.2\%$ at 6 h post-incubation. These results demonstrate that APT20TTMG is efficiently internalized by U-87 MG cells.

APT20TTMG alters viability and proliferation, and induces apoptosis in U-87 MG cells

A 31.4 \pm 1.8% (p = 0.0064) reduction in cell viability was observed after 48 h of treatment with 30 μ M APT20TTMG (Fig. 1a). This reduction persisted at 96 h, with 0.3, 3, and 30 μ M APT20TTMG significantly decreasing viability by 30.3 \pm 3.1% (p = 0.0185), 37.3 \pm 6.3% (p = 0.0045), and 66.2 \pm 1.2% (p < 0.0001), respectively. A similar trend was observed at 144 h, with reductions of 22.5 \pm 7.7% (p = 0.0481), 33.6 \pm 7.3% (p = 0.0038), and 71.9 \pm 4.1% (p < 0.0001) for 0.3, 3, and 30 μ M APT20TTMG, respectively. Cisplatin, a gold-standard cancer treatment, was tested under the same conditions. Its inhibitory concentration (IC₅₀) and I_{max} values for U-87 MG viability are summarized in Supplementary Table S1.

At 48 h, treatment with 0.03, 0.3, and 3 μ M APT20TTMG transiently increased cell proliferation by $13.1 \pm 0.9\%$ (p = 0.0332), $27.3 \pm 5.3\%$ (p = 0.0001), and $19.4 \pm 3.1\%$ (p = 0.0024), respectively (Fig. 1b). This early effect was not sustained, as no significant changes were observed at 96 h. However, at 144 h, all tested concentrations of APT20TTMG (0.003, 0.03, 0.3, 3, and 30 μ M) significantly decreased

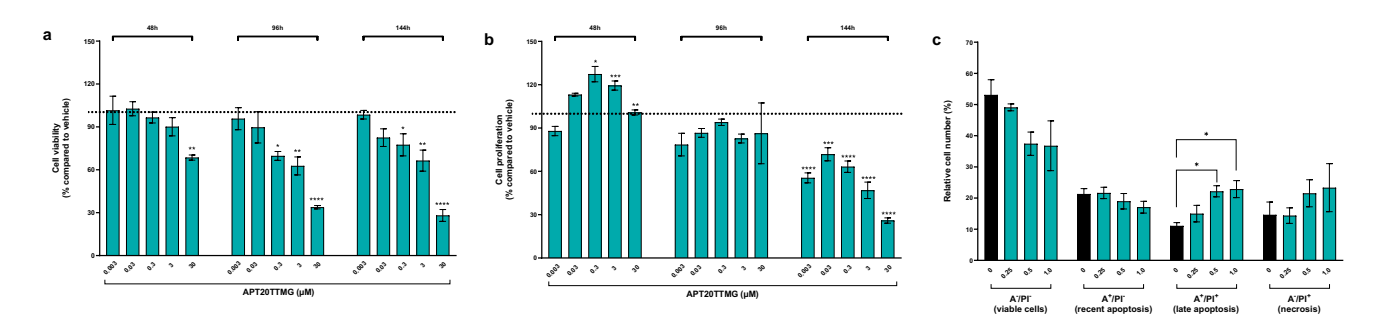


Fig. 1 APT20TTMG decreases the viability and proliferation of U-87 MG cells, and induces late apoptosis. Cells were treated with five concentrations of APT20TTMG (0.003, 0.03, 0.3, 3, and 30 μ M), and the **a** cell viability and **b** cell proliferation were evaluated by the MTT and BrdU assays, respectively, at 48, 96, and 144 h post treatment. Cells were treated with three concentrations of APT20TTMG (0.25, 0.5, and 1 μ M), and **c** apoptosis phases were evaluated 24 h after the treatment. Phases: A⁻/PI⁻ (viable cells); A⁺/PI⁻ (recent apopto-

sis); A^+/PI^+ (late apoptosis); A^-/PI^+ (necrosis). Data are plotted as a percentage of cell viability, cell proliferation, or apoptosis phases compared to non-treated cells. Results are expressed as mean \pm SEM of three independent experiments performed in three (graphs **a** and **b**) or two (graph **c**) technical replicates. One-way ANOVA, followed by Dunnett's multiple comparison test. *p<0.05, **p<0.01, ***p<0.001, and ****p<0.0001



Medical Oncology (2025) 42:507 Page 5 of 11 507

proliferation by 44.5 \pm 3.4% (p < 0.0001), 28.2 \pm 4.5% (p = 0.0008), 36.8 \pm 3.9% (p < 0.0001), 53.1 \pm 5.7% (p < 0.0001), and 74.1 \pm 1.8% (p < 0.0001), respectively. In contrast, cisplatin did not increase cell proliferation at any time point (Supplementary Table S2). APT20TTMG exhibited a concentration-dependent cytotoxic effect, with IC 50 decreasing from 62.3 μ M to 6.8 μ M and I max increasing from 31.4 \pm 3.1% to 71.9 \pm 7.2% over time. The sustained reduction in proliferation further indicates a cytostatic effect of APT20TTMG in U-87 MG cells.

Regarding apoptosis, 0.5 μ M and 1 μ M APT20TTMG significantly increased annexin V and propidium iodide positive cells (A⁺/PI⁺ markers) by 100.3 \pm 16.2% (p = 0.0170) and 106.8 \pm 24.5% (p = 0.0123) (Fig. 1c) respectively, indicating late apoptosis.

APT20TTMG exhibits antitumor activity in mice

Starting from day 16, both APT20TTMG and TMZ exhibited significant antitumor activity in the s.c. xenograft study, reducing the mean tumor volume by 46.5% (470.6 ± 67.6 , p = 0.0102) and 47.0% (466.5 ± 72.3 , p = 0.0094) (Fig. 2a), respectively, compared to the vehicle group. APT20TTMG

showed superior efficacy on days 20 (46.7% reduction; 640.9 ± 129.1 , p = 0.0002) and 22 (42% reduction; 843.1 ± 192.3 , p < 0.0001), whereas TMZ achieved its maximum inhibition on day 16, with reduced efficacy thereafter. On day 20, APT20TTMG reduced the tumor volume ratio (tumor volume/growth inhibition) by 50.1% (6.4 ± 1.3 , p = 0.0016), compared to the vehicle group, outperforming TMZ (43.5% reduction; 7.2 ± 2.0 , p = 0.0072) (Fig. 2b). By day 22, APT20TTMG maintained a greater reduction (43.5%; 8.6 ± 2.1 , p = 0.0010) than TMZ (33.1%; 10.2 ± 2.8 , p = 0.0170). Although TMZ also reduced the ratio on day 16 (4.6 ± 0.8 , p = 0.0388; vehicle: 9.0 ± 1.4), APT20TTMG exhibited higher maximum inhibition at the end of the evaluation period (days 20 and 22).

Analysis of the area under the curve (AUC) for tumor growth revealed that APT20TTMG and TMZ decreased the total area by 41.3% (8244 ± 1207 , p = 0.0214) and 38.6% (8619 ± 1292 , p = 0.0316) (Fig. 2c), respectively, compared to the vehicle group. Although not statistically significant, APT20TTMG showed a trend toward a 36.8% reduction in tumor weight, while TMZ showed a 26.9% reduction (Fig. 2d). Notably, APT20TTMG, but not TMZ, tended to increase both absolute and relative body weights (Fig. 2e–f,

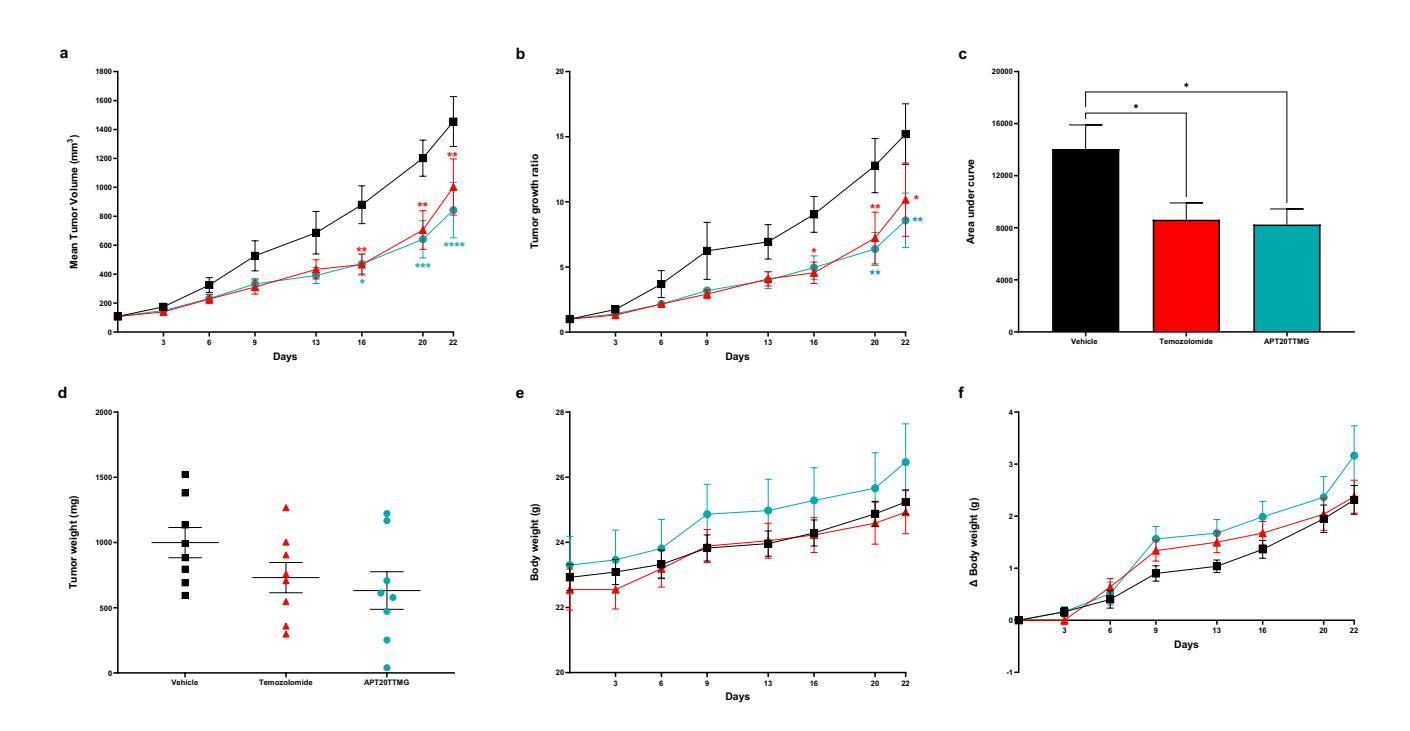


Fig. 2 APT20TTMG decreases tumor volume in a s.c. xenograft glioblastoma model. U-87 MG tumors were implanted in experimental animals via s.c. Once the tumor reached approximately 100 mm³, animals were divided into groups and treated with saline (5 ml/kg of saline, i.v.), TMZ (5 mg/kg, p.o), or APT20TTMG (20 mg/kg, i.v.) for 22 days. Tumor volume and body weight were measured twice a week. **a** Mean tumor volume (mm³) over time. **b** Tumor growth ratio calculated as tumor volume at each time point relative to the initial volume at day 0. **c** Area under the curve (AUC) derived from tumor

volume over the treatment period. **d** Tumor weight at the end of treatment. **e** Absolute body weight measured throughout the experiment. **f** Relative body weight, expressed as percentage of the weight at the start of treatment. Data are expressed as mean \pm SEM (n=8/group). Two-way ANOVA, followed by Tukey's post hoc test (graphs **a**, **b**, **d**, and **e**), and one-way ANOVA, followed by Dunnett's multiple comparison test (graphs **c** and **f**). *p<0.05, **p<0.01, ***p<0.001,



507 Page 6 of 11 Medical Oncology (2025) 42:507

respectively), which may indicate a favorable tolerability profile in treated animals.

APT20TTMG induces histopathological tumor changes

Elevated Ki-67 levels in cancer cells indicate a poorly differentiated and potentially more aggressive tumor. Although no statistical differences were observed among treated groups, APT20TTMG decreased Ki-67-positive cells by 14.6% (7.7 ± 1.4), when compared to the vehicle group (9.1 ± 1.7) (Supplementary Fig. S2a). This effect was comparable to TMZ, which reduced Ki-67-positive cells by 17.5% (7.5 ± 1.1), indicating that APT20TTMG has a proliferative index similar to the standard GBM treatment. Moreover, tumors in the APT20TTMG and TMZ groups exhibited fewer anaplastic features and cellular atypia, extensive mixed-type infiltrate, and prominent central necrosis, compared to the vehicle group (Supplementary Fig. S2b).

The nucleus-to-cytoplasm ratio (N:C), an indicator of cellular dedifferentiation, was reduced by treatment with APT20TTMG (Supplementary Fig. S3a and Supplementary Fig. S4), with 50% of animals displaying a low ratio, 33.3% intermediate, and 16.7% high. In contrast, TMZ-treated animals exhibited only intermediate ratios, while the vehicle

group showed 12.5% low, 50% intermediate, and 37.5% high ratios. APT20TTMG also increased apoptosis (66.67% mild and 33.33% moderate), compared to the vehicle (100% mild) and TMZ (87.5% mild and 12.5% moderate) groups (Supplementary Fig. S3b). The presence of prominent necrosis was lower in the APT20TTMG group (66.7%) when compared to TMZ (75%) and vehicle (87.5%) groups (Supplementary Fig. S3c).

Less differentiated cells (more malignant) are less likely to form a capsule, which reduces tumor migration and invasion. APT20TTMG-treated animals had the highest capsule formation (83.3%), compared to TMZ (75%) and vehicle (37.5%) groups (Supplementary Fig. S3d). Angiogenesis analysis revealed mild levels in 66.7% of APT20TTMGtreated animals, unlike vehicle and TMZ groups, where only 37.5% showed mild angiogenesis (Supplementary Fig. S3e). Differentiation assessment demonstrated that APT20TTMGtreated animals were the only ones to present cells with Grade 1 differentiation (16.7%), followed by 66.7% in Grade 2 and 16.7% in Grade 3 (Supplementary Fig. S3f). Vehicle and TMZ groups only presented cells in Grade 2 (50% and 62.5%, respectively) and Grade 3 (50% and 37.5%, respectively). Although APT20TTMG-treated animals exhibited favorable distributions across these histopathological parameters, no statistical differences were observed.

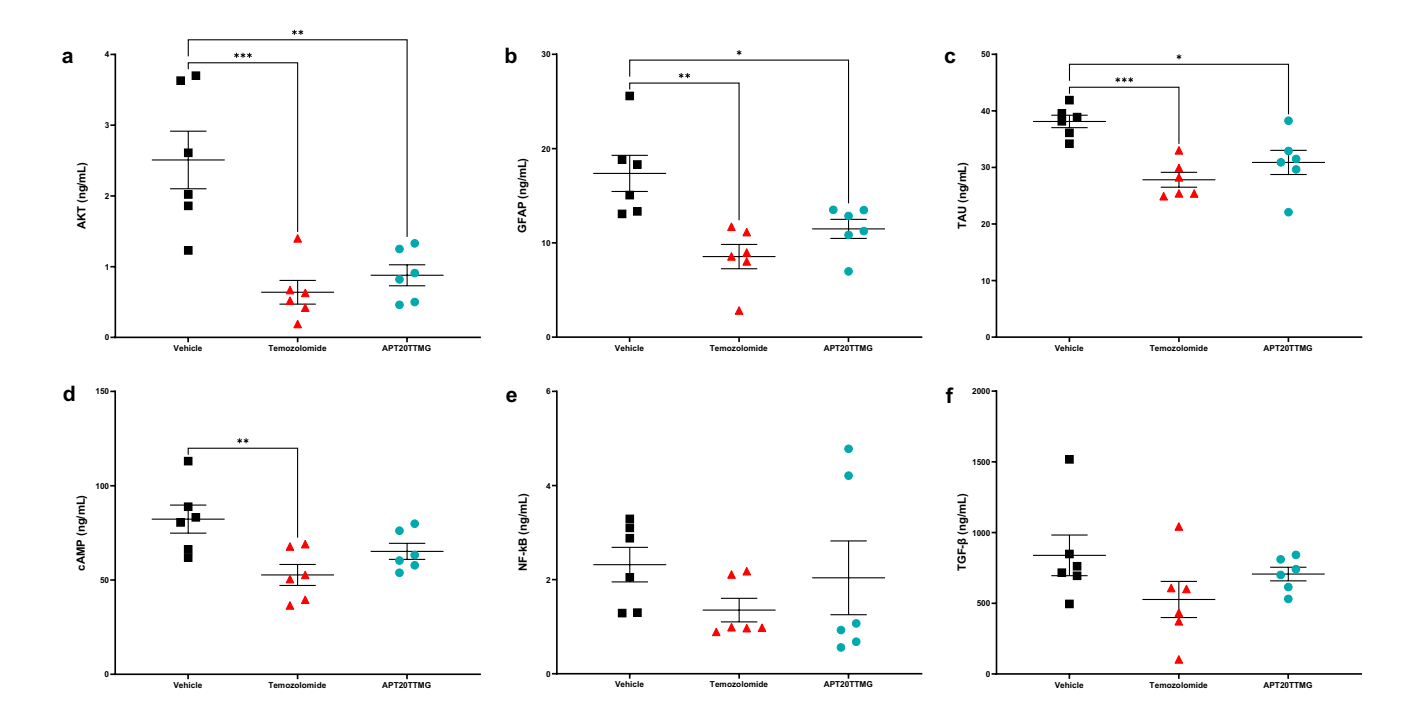


Fig. 3 Oncogenic signaling pathways are modulated by APT20TTMG in a s.c. xenograft glioblastoma model. U-87 MG tumors were implanted in experimental animals via s.c. Once the tumor reached approximately 100 mm³, animals were divided into groups and treated with saline (5 ml/kg of saline, i.v.), TMZ (5 mg/kg, p.o), or APT20TTMG (20 mg/kg, i.v.) for 22 days. In the end of

the treatments, animals were euthanized and tumor tissues were processed for the evaluation of oncogenic signaling pathways by ELISA. **a** AKT. **b** GFAP. **c** TAU. **d** cAMP. **e** NF-kB. **f** TGF- β . Data are presented as individual values of protein quantification (ng/ml) (n=6/group). One-way ANOVA, followed by Dunnett's multiple comparison test. *p < 0.01, **p < 0.01, and ***p < 0.001



Medical Oncology (2025) 42:507 Page 7 of 11 507

APT20TTMG decreases GBM biomarkers

To identify signaling pathways activated by APT20TTMG, some biomarkers were analyzed in U-87 MG tumors. APT20TTMG reduced AKT levels by 65% (0.9 ± 0.1, p = 0.0012), compared to the vehicle group (2.5 ± 0.4) (Fig. 3a). A similar reduction was observed with TMZ $(74.6\%; 0.6 \pm 0.2)$, suggesting that APT20TTMG disrupts cancer cell growth and survival by affecting AKT-regulated cellular processes, such as proliferation and survival. GFAP, a marker of glial tumors, was reduced by 33.9% with APT20TTMG (11.5 \pm 1.0, p = 0.0223) and by 50.8% with TMZ $(8.5 \pm 1.3, p = 0.0013)$, compared to the vehicle group (Fig. 3b). TAU levels were also significantly reduced by APT20TTMG (19%; 30.9 ± 2.1 , p = 0.0103) and TMZ $(27\%; 27.8 \pm 1.3, p = 0.0007)$ (Fig. 3c), supporting its role in cancer progression. Although TMZ reduced cAMP by 36% $(52.7 \pm 5.6, p = 0.0056)$, no statistically significant difference was observed in the APT20TTMG group (20.8% reduction; 65.2 ± 4.3) (Fig. 3d). Also, no significant changes were observed in NF-kB and TGF-β levels for either treatment (Fig. 3e-f, respectively). Overall, these findings suggest that APT20TTMG affects classical GBM pathways (AKT), and emerging mechanisms including microtubule alteration (TAU) and astrogliosis (GFAP).

APT20TTMG, alone and in combination with TMZ, stops tumor progression

A pilot xenograft study was conducted to evaluate a possible synergic effect between APT20TTMG and TMZ. One day after the first attack dose (day 8) of the pilot study, a significant reduction in tumor volume was observed in the 20 mg/kg APT20TTMG+TMZ group $(43.1\%; 218.4 \pm 18.06, p = 0.0215)$, compared to the vehicle group (Fig. 4a). This reduction persisted on day 10 $(46.5\%; 265.3 \pm 17.2, p = 0.0003)$. On this same day, significant decreases were also observed in the 20 mg/kg APT20TTMG (38.2%; 306.2 \pm 25.4, p = 0.0053) and 10 mg/ kg APT20TTMG+TMZ (34.9%; 322.8 \pm 23.7, p = 0.0142) groups, compared to the vehicle group. By day 12, reductions further improved to 48.1% (321.4 ± 17.2, p < 0.0001), 41.7% (360.7 ± 27.5, p = 0.0142), and 38.1% (383.1 ± 31.6, p < 0.0001) in these groups, respectively. Additionally, the 10 mg/kg APT20TTMG group showed a 28.8% reduction $(440.5 \pm 24.8, p = 0.0104)$. These effects persisted until day 22, with reductions of 63.4% (579.8 \pm 39.7) for 20 mg/kg APT20TTMG + TMZ, 48.2% (817.4 ± 78.9) for 20 mg/kg APT20TTMG, 46.1% (851.2 ± 23.3) for 10 mg/ kg APT20TTMG + TMZ, and 30.0% (1104.8 \pm 86.0) for 10 mg/kg APT20TTMG (p < 0.0001 for all groups). Tumor volume curves plateaued by day 26, except for the 10 mg/ kg APT20TTMG group, suggesting effective tumor growth control with higher doses of APT20TTMG, alone or combined with TMZ.

Regarding tumor growth ratio, on day 10, only the 20 mg/kg APT20TTMG+TMZ group showed a 44.5% reduction $(3.4 \pm 0.3, p = 0.0182)$, compared to the vehicle group (Fig. 4b). By day 12, reductions were 45.9% $(4.1 \pm 0.3, p = 0.0008)$ for 20 mg/kg APT20TTMG+TMZ, 41.3% (4.5 ± 0.3, p = 0.0034) for 20 mg/kg APT20TTMG, and 37.2% (4.8 ± 0.4, p = 0.0118) for 10 mg/kg APT20TTMG+TMZ group. By day 15, the tumor growth ratio decreased further, showing reductions of 52.7% $(5.4 \pm 0.5, p < 0.0001)$ for 20 mg/kg APT20TTMG+TMZ, 48.2% (5.9 ± 0.3, p < 0.0001) for 20 mg/kg APT20TTMG, 42% $(6.6 \pm 0.6, p < 0.0001)$ for 10 mg/kg APT20TTMG+TMZ, and 30.8% $(7.9 \pm 0.8, p = 0.0007)$ for 10 mg/kg APT20TTMG. These effects persisted until day 22, with reductions of 61.6% (7.4 ± 0.7), 48.1% (10.0 ± 0.7), 43.3% (11.0 ± 1.4), and 28.7% (13.8 ± 1.0), respectively (p < 0.0001 for all groups). The AUC and tumor weight data (Fig. 4c-d, respectively) further supported these findings. The 20 mg/kg APT20TTMG+TMZ and 10 mg/kg APT20TTMG+TMZ groups showed AUC reductions of 52.7% (6733 \pm 282.5, p < 0.0001) and 39.8% (8572 \pm 309.2, p < 0.0001), respectively, and tumor weight reductions of 53% (520.00 ± 20.5 , p < 0.0001) and 31.9% (754.3 ± 25.5 , p = 0.0007), respectively, compared to the vehicle group (AUC: $14,252 \pm 650$; tumor weight: 1107.4 ± 48.7). Alone, both doses reduced AUC by 43.4% (8060 ± 444.5 , p < 0.0001) and 28.4% (10,199 ± 394.6, p < 0.0001) and tumor weight by 46.7% (589.7 ± 40.0 , p < 0.0001) and 22.3% (860.3 \pm 57.5, p = 0.0112), respectively. No changes in body weight (Fig. 4e-f) or clinical signs were observed. Therefore, APT20TTMG, particularly at 20 mg/kg alone or combined with TMZ, demonstrated significant effects in reducing tumor volume and growth in the xenograft model.

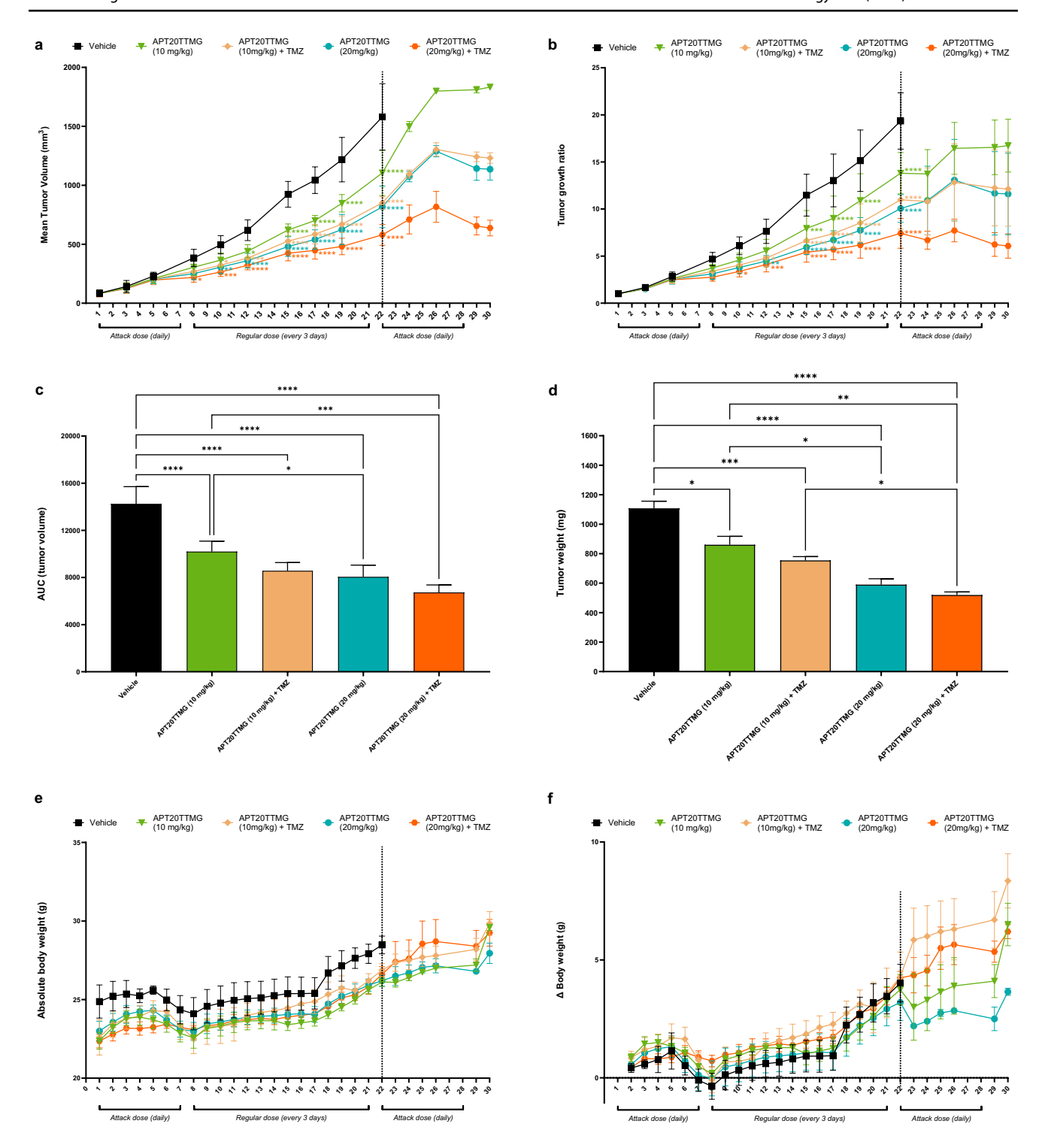
Discussion

This study proposes that APT20TTMG, a novel synthetic cDNA, exhibits an effective mechanism against GBM. We have previously demonstrated the therapeutic correction of the U1 snRNP complex by APT20TTMG [20]. As the spliceosome machinery has been demonstrated to be altered in GBM [16], APT20TTMG represents a potential therapeutic strategy, although further studies are required to evaluate its efficacy and safety.

As previously described [20], to achieve its mechanism of action, APT20TTMG was specifically designed to contain a sequence complementary to highly conserved regions at exon–intron donor splicing sites in pre-mRNAs. It also features a secondary structure and chemical modifications that facilitate interactions with U1-C and U1-70K



507 Page 8 of 11 Medical Oncology (2025) 42:507



proteins, modulating their distance, position, and behavior to ensure proper snRNP assembly. Upon entering the nucleus, APT20TTMG binds to the donor splicing sites, effectively displacing the RNA-binding domain of U1 snRNA. This interaction, along with the attraction of U1 snRNPs, ensures correct positioning and initiation of splicing, even under pathological conditions.

The assembly of the U1 snRNP complex, regulated by U1-70K, controls the availability of Sm proteins, which are shared among spliceosome snRNPs, thereby influencing the cellular snRNP repertoire [18]. Elevated levels of SmG, an Sm protein, have been associated with TMZ resistance and the regulation of p53 and Myc pathways, which are critical for cell cycle progression in GBM [16]. SmG availability,



Medical Oncology (2025) 42:507 Page 9 of 11 507

√Fig. 4 The combination of APT20TTMG with TMZ has enhanced antitumoral activity in a pilot s.c. xenograft glioblastoma model study. U-87 MG tumors were implanted in experimental animals via s.c. Once the tumor reached approximately 100 mm³, animals were divided into groups and treated with saline (5 ml/kg of saline, i.v.), APT20TTMG (10 or 20 mg/kg, i.v.), or APT20TTMG (10 or 20 mg/kg, i.v.)+TMZ (5 mg/kg, p.o) for 30 days. During the first seven days and the last seven days, animals received a daily attack dose of APT20TTMG. From days eight to 21, animals received a regular dose of APT20TTMG every three days. Tumor volume was measured twice a week, and body weight and clinical signs were measured daily. All the vehicle animals and three animals from each treatment group were euthanized on the 22nd day, and the remaining animals continued in the study until the 30th day. a Mean tumor volume (mm³) over time. **b** Tumor growth ratio calculated as tumor volume at each time point relative to the initial volume at day 0. c Area under the curve (AUC) derived from tumor volume over the treatment period. d Tumor weight at the end of treatment. e Absolute body weight measured throughout the experiment. f Relative body weight, expressed as percentage of the weight at the start of treatment. Data are expressed as mean \pm SEM (n=3-5/group). Two-way ANOVA, followed by Tukey's post hoc test (graphs a, b, e, and f), and oneway ANOVA, followed by Tukey's post hoc test (graphs c and d). *p < 0.05, **p < 0.01, ***p < 0.001, and ****p < 0.0001

regulated by U1 snRNP assembly, may also play a key role in GBM physiopathology and therapy resistance. By promoting proper U1 snRNP assembly [20], APT20TTMG prevents premature polyadenylation of pre-mRNAs and may positively influence SmG availability, leading to cell cycle arrest.

The cellular uptake of molecules similar to APT20TTMG, such as aptamers and oligonucleotides, typically involves initial adsorption followed by endocytic pathways [21–23]. Rapidly growing cells exhibit higher oligonucleotide uptake efficiency compared to slow-growing cells [24], which may explain the increased APT20TTMG internalization of 63.6% at 6 h. This efficient and sustained internalization is crucial for the beneficial effects demonstrated in this study. These effects include APT20TTMG's ability to induce cell death and suppress proliferation in U-87 MG, highlighting its potential for controlled cancer growth inhibition.

Xenograft models effectively simulate human tumor progression [25]. U-87 MG cells, known to be more sensitive to TMZ [26], are one of the most extensively characterized and widely used GBM cell lines. They offer significant advantages, including the ability to perform direct comparisons across studies and enhance experimental reproducibility. Their well-defined characteristics also facilitate reliable in vitro assays and subsequent in vivo validations, making them a robust tool for preclinical research [27]. We observed that APT20TTMG was more effective than TMZ in decreasing tumor volume and promoting weight gain. Considering that GBM patients frequently experience weight loss as a consequence of the heterogeneous tumor metabolism [28, 29], APT20TTMG could also play a role in metabolic

regulation. Additionally, the reduction in tumor volume aligns with APT20TTMG's ability to induce apoptosis in U-87 MG cells, a critical feature of cancer therapy that promotes targeted cell death with minimal tissue damage [30]. This apoptotic effect probably involves phosphatidylserine translocation, triggering downstream apoptotic pathways and membrane permeabilization, further contributing to tumor suppression [31].

Combination therapies often enhance outcomes by leveraging complementary mechanisms. The beneficial effects observed with 10 or 20 mg/kg APT20TTMG combined with TMZ suggest improved antitumor activity. This may be attributed to APT20TTMG's ability to restore U1 snRNP function and normalize SmG availability [20], potentially overcoming TMZ resistance and p53 and Myc pathways [16]. Further studies are needed to fully explore these benefits and optimize this combination.

Moreover, treatment with APT20TTMG reduced key biomarkers associated with GBM: AKT, which promotes tumor survival [32], GFAP, elevated in reactive astrogliosis and linked to pro-tumor effects [33, 34], and TAU, implicated in cancer through its role in p53 regulation and DNA repair and decreased cell motility and migration of U-87 MG cells [35–37]. The reduction of AKT, GFAP, and TAU by APT20TTMG, comparable to TMZ, suggests it may mitigate reactive astrogliosis, counteract the immunosuppressive environment, and inhibit cell proliferation. While the significant reduction of these biomarkers is consistent with our proposed U1 snRNP-mediated mechanism based on prior mechanistic studies, they represent correlative evidence rather than proof of direct causality between APT20TTMG's splicing modulation and specific protein reduction. Future studies involving APT20TTMG's effects on U1 snRNP function and subsequent splicing alterations in GBM cells are needed to establish a direct causal relationship.

In conclusion, APT20TTMG represents a promising therapeutic candidate for GBM due to its unique mechanism of modulating pre-mRNA splicing and suppressing premature polyadenylation. Preliminary studies suggest that APT20TTMG exhibits a high degree of specificity in its mechanism of action, with no off-target effects observed so far. However, further comprehensive studies are essential to rigorously evaluate its selectivity and potential toxicities, given the ubiquitous role of U1 snRNP in mRNA processing. Such investigations should be performed in more complex and clinically relevant models, such as patient-derived cell lines and orthotopic GBM models that more accurately recapitulate the tumor microenvironment, genetic heterogeneity, and therapeutic resistance observed in humans. These additional studies will be critical to confirm the absence of off-target activity and to ensure the safety and efficacy of APT20TTMG before advancing to clinical development.



507 Page 10 of 11 Medical Oncology (2025) 42:507

Supplementary Information The online version contains supplementary material available at https://doi.org/10.1007/s12032-025-03057-w.

Acknowledgement The authors are thankful for Vesper Biotechnologies, LP (Delaware, US), for providing venture capital that enabled the execution of the experiments.

Author contributions All authors contributed to the study conception and design. CBQdSL: conceived the original idea for the study, analyzed data, interpreted the results, and wrote the first draft of the manuscript. CGMZ, VdVCS, and ESS: collected and analyzed data, interpreted results and contributed to drafts of the manuscript. MSR and RMB: interpreted results and contributed to drafts of the manuscript. All authors read and approved the final manuscript.

Funding The authors have not disclosed any funding.

Data availability The datasets generated and analyzed during the current study are available from the corresponding author on reasonable request.

Declarations

Conflict of interest Financial interests: Caio Bruno Quinta de Souza Leal has filed a patent related to this work (US11946050B2). Camila Guimarães Moreira Zimmer, Vanessa de Vasconcelos Castilho Sinatti, and Ericks Sousa Soares are employees of Aptah Bio Inc. Caio Bruno Quinta de Souza Leal and Rafael Mantovani Bottos are co-founders of Aptah Bio Inc. Michael S. Rafii is a member of the scientific advisory board of Aptah Bio Inc.

Ethical approval This study was approved by the Institutional Animal Ethics Committee of Dabur Research Foundation (approval number: IAEC/79/1532) and authorized by the Committee for the Purpose of Control and Supervision of Experiments on Animals of India (registration no. 64/PO/RcBi/S/99/CPCSEA).

References

- Hanif F, Muzaffar K, Perveen K, Malhi SM, Simjee SU. Glioblastoma multiforme: a review of its epidemiology and pathogenesis through clinical presentation and treatment. Asian Pac J Cancer Prev. 2017;18:3–9.
- Louis DN, Perry A, Wesseling P, Brat DJ, Cree IA, Figarella-Branger D, et al. The 2021 WHO classification of tumors of the central nervous system: a summary. Neuro Oncol. 2021;23:1231-51.
- Sevastre A-S, Costachi A, Tataranu L, Brandusa C, Artene S, Stovicek O, et al. Glioblastoma pharmacotherapy: a multifaceted perspective of conventional and emerging treatments (Review). Exp Ther Med. 2021;22:1408.
- Liu S, Cadoux-Hudson T, Schofield CJ. Isocitrate dehydrogenase variants in cancer—cellular consequences and therapeutic opportunities. Curr Opin Chem Biol. 2020;57:122–34.
- Melhem JM, Detsky J, Lim-Fat MJ, Perry JR. Updates in IDHwildtype glioblastoma. Neurotherapeutics. 2022;19:1705–23.
- Nam Y, Koo H, Yang Y, Shin S, Zhu Z, Kim D, et al. Pharmacogenomic profiling reveals molecular features of chemotherapy resistance in IDH wild-type primary glioblastoma. Genome Med. 2023;15:16.
- Smith HL, Wadhwani N, Horbinski C. Major features of the 2021 WHO classification of CNS tumors. Neurotherapeutics. 2022;19:1691–704.

- 8. Chu Y, Elrod N, Wang C, Li L, Chen T, Routh A, et al. Nudt21 regulates the alternative polyadenylation of Pak1 and is predictive in the prognosis of glioblastoma patients. Oncogene. 2019;38:4154–68.
- Masamha CP, Xia Z, Yang J, Albrecht TR, Li M, Shyu A-B, et al. CFIm25 links alternative polyadenylation to glioblastoma tumour suppression. Nature. 2014;510:412–6.
- Mayr C, Bartel DP. Widespread shortening of 3'UTRs by alternative cleavage and polyadenylation activates oncogenes in cancer cells. Cell. 2009;138:673–84.
- 11. Xia Z, Donehower LA, Cooper TA, Neilson JR, Wheeler DA, Wagner EJ, et al. Dynamic analyses of alternative polyadenylation from RNA-seq reveal a 3'-UTR landscape across seven tumour types. Nat Commun. 2014;5:5274.
- Yuan F, Hankey W, Wagner EJ, Li W, Wang Q. Alternative polyadenylation of mrna and its role in cancer. Genes Dis. 2021;8:61-72.
- 13. Fu Y, Sun Y, Li Y, Li J, Rao X, Chen C, et al. Differential genome-wide profiling of tandem 3' UTRs among human breast cancer and normal cells by high-throughput sequencing. Genome Res. 2011;21:741–7.
- Bai B. U1 snRNP alteration and neuronal cell cycle reentry in Alzheimer disease. Front Aging Neurosci. 2018;10:75.
- Fuentes-Fayos AC, Vázquez-Borrego MC, Jiménez-Vacas JM, Bejarano L, Pedraza-Arévalo S, L.-López F, et al. Splicing machinery dysregulation drives glioblastoma development/aggressiveness: oncogenic role of SRSF3. Brain. 2020;143:3273-93.
- Lan Y, Lou J, Hu J, Yu Z, Lyu W, Zhang B. Downregulation of SNRPG induces cell cycle arrest and sensitizes human glioblastoma cells to temozolomide by targeting Myc through a p53-dependent signaling pathway. Cancer Biol Med. 2020;17:112-31.
- Oh J-M, Venters CC, Di C, Pinto AM, Wan L, Younis I, et al. U1 snrnp regulates cancer cell migration and invasion in vitro. Nat Commun. 2020;11:1.
- So BR, Wan L, Zhang Z, Li P, Babiash E, Duan J, et al. A U1 snRNP-specific assembly pathway reveals the SMN complex as a versatile hub for RNP exchange. Nat Struct Mol Biol. 2016;23:225-30.
- Venters CC, Oh J-M, Di C, So BR, Dreyfuss G. U1 snRNP telescripting: suppression of premature transcription termination in introns as a new layer of gene regulation. Cold Spring Harb Perspect Biol. 2019;11:a032235.
- Leal CBQS, Zimmer CGM, Sinatti VVC, Soares ES, Poppe B, de Wiart AC, et al. Effects of the therapeutic correction of U1 snRNP complex on Alzheimer's disease. Sci Rep. 2024;14:30085.
- Alamudi SH, Kimoto M, Hirao I. Uptake mechanisms of cellinternalizing nucleic acid aptamers for applications as pharmacological agents. RSC Med Chem. 2021;12:1640–9.
- Yoon S, Rossi JJ. Aptamers: uptake mechanisms and intracellular applications. Adv Drug Deliv Rev. 2018;134:22–35.
- Zhang R, Qin X, Kong F, Chen P, Pan G. Improving cellular uptake of therapeutic entities through interaction with components of cell membrane. Drug Deliv. 2019;26:328–42.
- Crooke ST, Wang S, Vickers TA, Shen W, Liang X. Cellular uptake and trafficking of antisense oligonucleotides. Nat Biotechnol. 2017;35:230–7.
- Schmidt KM, Geissler EK, Lang SA. Subcutaneous murine xenograft models: a critical tool for studying human tumor growth and angiogenesis in vivo. Methods Mol Biol. 2016;1464:129–37.
- Lee SY. Temozolomide resistance in glioblastoma multiforme. Genes Dis. 2016;3:198–210.
- Schulz JA, Rodgers LT, Kryscio RJ, Hartz AMS, Bauer B. Characterization and comparison of human glioblastoma models. BMC Cancer. 2022;22:844.



Medical Oncology (2025) 42:507 Page 11 of 11 507

 Bernhard C, Reita D, Martin S, Entz-Werle N, Dontenwill M. Glioblastoma metabolism: insights and therapeutic strategies. Int J Mol Sci. 2023;24:9137.

- Bertoli S, Battezzati A, Petruzzi A, Leone A, De Amicis R, Tramacere E, et al. Anthropometrics and body composition in adults with high-grade gliomas: effects of disease-related variables. Nutr Cancer. 2018;70:431–40.
- Carneiro BA, El-Deiry WS. Targeting apoptosis in cancer therapy. Nat Rev Clin Oncol. 2020;17:395

 –417.
- Galluzzi L, Vitale I, Aaronson SA, Abrams JM, Adam D, Agostinis P, et al. Molecular mechanisms of cell death: recommendations of the nomenclature committee on cell death 2018. Cell Death Differ. 2018;25:486–541.
- 32. He Y, Sun MM, Zhang GG, Yang J, Chen KS, Xu WW, et al. Targeting PI3K/Akt signal transduction for cancer therapy. Signal Transduct Target Ther. 2021;6:425.
- Nieland L, Morsett LM, Broekman MLD, Breakefield XO, Abels ER. Extracellular vesicle-mediated bilateral communication between glioblastoma and astrocytes. Trends Neurosci. 2021;44:215–26.
- 34. Uceda-Castro R, van Asperen JV, Vennin C, Sluijs JA, van Bodegraven EJ, Margarido AS, et al. GFAP splice variants fine-tune glioma cell invasion and tumour dynamics by modulating migration persistence. Sci Rep. 2022;12:424.

- Callari M, Sola M, Magrin C, Rinaldi A, Bolis M, Paganetti P, et al. Cancer-specific association between Tau (MAPT) and cellular pathways, clinical outcome, and drug response. Sci Data. 2023:10:637.
- 36. Breuzard G, Pagano A, Bastonero S, Malesinski S, Parat F, Barbier P, et al. Tau regulates the microtubule-dependent migration of glioblastoma cells via the Rho-ROCK signaling pathway. J Cell Sci. 2019;132:jcs222851.
- 37. Pagano A, Breuzard G, Parat F, Tchoghandjian A, Figarella-Branger D, De Bessa TC, et al. Tau regulates glioblastoma progression, 3D cell organization, growth and migration via the PI3K-AKT axis. Cancers. 2021;13:5818.

Publisher's Note Springer Nature remains neutral with regard to jurisdictional claims in published maps and institutional affiliations.

Springer Nature or its licensor (e.g. a society or other partner) holds exclusive rights to this article under a publishing agreement with the author(s) or other rightsholder(s); author self-archiving of the accepted manuscript version of this article is solely governed by the terms of such publishing agreement and applicable law.

